

Strongly correlated physics in organic open-shell quantum systems

G. Gandus,^{1,*} D. Passerone,² R. Stadler,³ M. Luisier,¹ and A. Valli^{3,4,†}

¹*Integrated Systems Laboratory, ETH Zürich, Gloriastrasse 35, 8092 Zürich, Switzerland*

²*Empa, Swiss Federal Laboratories for Materials Science and Technology, Überlandstrasse 129, CH-8600, Dübendorf, Switzerland*

³*Institute for Theoretical Physics, Vienna University of Technology, Wiedner Hauptstrasse 8-10, A-1040 Vienna, Austria*

⁴*Department of Theoretical Physics, Institute of Physics, Budapest University of Technology and Economics, Műegyetem rkp. 3., H-1111 Budapest, Hungary*

Strongly correlated physics arises due to electron-electron scattering within partially-filled orbitals, and in this perspective, organic molecules in open-shell configuration are good candidates to exhibit many-body effects. With a focus on neutral organic radicals with a molecular orbital hosting a single unpaired electron (SOMO) we investigate many-body effects on electron transport in a single-molecule junction setup. Within a combination of density functional theory and many-body techniques, we perform numerical simulations for an effective model for which all the parameters, including the Coulomb tensor, are derived *ab-initio*. We demonstrate that the SOMO resonance is prone towards splitting, and identify a *giant* electronic scattering rate as the driving many-body mechanism, akin to a Mott metal-to-insulator transition. The nature of the splitting, and thus of the resulting gap, as well as the spatial distribution of the SOMO and its coupling to the electrodes, have dramatic effects on the transport properties of the junction. We argue that the phenomenon and the underlying microscopic mechanism are general, and apply to a wide family of open-shell molecular systems.

I. INTRODUCTION

Strongly correlated electronic physics arises in partially occupied orbitals in the presence of competing energy scales. Due to the Coulomb repulsion, electrons display a collective behavior, leading to the breakdown of the single-particle picture and the emergence of complex quantum phenomena. Electronic correlations are also enhanced due to spatial confinement effects in low-dimensional and nanoscopic systems. While in solid-state physics the concept of a “strongly-correlated metal” is well-established, its analog for molecules is not obvious.

In chemistry, the majority of stable organic molecules have closed-shell electronic configurations, and electrons are paired in delocalized molecular orbitals (MOs) that are either completely filled or empty. The energy difference between the frontier MOs, i.e., the highest occupied (HOMO) and the lowest unoccupied (LUMO) orbitals defines the spectral gap. In particular, π -conjugated systems display a wide HOMO-LUMO gap ($\Delta \sim \text{eV}$) which is controlled by the overlap of neighboring p_z orbitals. A molecular system in an open-shell configuration (radical) is characterized by unpaired valence electrons residing in non-bonding singly-occupied MOs (SOMOs) found at intermediate energies between HOMO and LUMO. Radicals can form by breaking bonds or by adding/removing electrons (e.g., in photoinduced processes) and are intermediate products of chemical reactions.

While open-shell configurations are typically associated with high chemical reactivity, there exist also species

of relatively stable radicals, which possess interesting electronic, magnetic, and optical functionalities that are relevant to technological applications ranging from next-generation spintronics to quantum information [1–3].

Tremendous advances in the synthesis and characterization of organic radicals triggered recent experimental studies with organic species that are stable enough to be trapped in break-junctions [4, 5] or investigated with scanning tunneling spectroscopy [6–9], which fueled a revival of interest in the molecular Kondo effect [4, 6–12]. There is a growing experimental and theoretical effort to unravel how many-body effects can dramatically influence electronic and transport properties in light of technological applications. In the context of molecular electronics, noteworthy organic radicals include triphenylmethyl [4, 5, 12], Blatter radical [13], polyacetylene [14, 15], benzyl [16, 17], together with the whole family of polycyclic hydrocarbons with non-Kekulé structure [7, 18–20]. Molecular organic frameworks with transition-metal centers (e.g., iron-porphyrin) are also typically open-shell, and have been recently suggested as molecular transistors [21, 22].

From the theoretical point of view, in wide-gap semiconductors, the electron-electron scattering rate is low due to the lack of electronic states at the Fermi energy. The accuracy of *ab-initio* prediction of the gap is a longstanding issue [23], and numerical simulations for insulators [24, 25] and molecules [25–32] predict a many-body renormalization of the spectral gap. However, these effects do not change qualitatively the transport properties. In open-shell configurations instead, it can be expected that electron-electron scattering within the partially filled SOMO and many-body effects have a prominent role.

* gandusgui@gmail.com

† valli.angelo@ttk.bme.hu

In computational quantum chemistry, it is well-established that open-shell molecular configurations require careful treatment (see, e.g., [33] for an overview) but the accuracy of quantum chemical methods comes at a high numerical cost. Hence, we recently witnessed significant advances in developing alternative simulation schemes, that are suitable to describe complex devices relevant to molecular electronics [11, 34, 35]. In the endeavor to achieve predictive power and allow for a quantitative comparison with experiments, a suitable method should be *high-throughput* — i.e., scalable and automated as much as possible, and able to describe a realistic chemical environment and many-body correlations within an *ab-initio* framework. This would allow a cooperative effort between theory and experiments, and pave the path to future breakthroughs for next-generation quantum technologies.

II. SCOPE OF THIS WORK

The scope of this work is to investigate the emergence of strongly correlated electron physics in the electronic and transport properties of single-molecule junctions.

To this end, we have developed a comprehensive numerical workflow that combines density functional theory (DFT) with quantum field theoretical methods, and it is able to address the complexity of a realistic chemical environment as well as electronic correlation effects beyond the single-particle picture within an *ab-initio* framework. With both aspects taken into account, we are able to unravel the origin of many-body transport effects in single-molecule junctions.

The art of combining *ab-initio* and many-body computational schemes lies in a transformation from non-orthogonal atomic orbitals (AOs) to recently introduced local orbitals (LOs) [36]. The LOs are by construction orthogonal within the same atom and localized in space. They take over the symmetries of the original AOs, while inheriting the information of the environment. This allows to represent the electronic wavefunction in a region of the spectrum close to the Fermi energy with a minimal set of orbitals, making them an ideal basis for many-body calculations. So far, LOs have been employed in the context of DFT [36]. In what follows, we also evaluate the Coulomb integrals that describe the electron-electron repulsion in the LO basis, and thus map to the original Hamiltonian onto an effective many-body problem, which we can feasibly solve with appropriate numerical methods. This recipe is particularly suitable to address strong correlation effects in the transport properties of molecular junctions.

In terms of applications, we focus on molecular break-junctions in which the central molecule bridging the electrodes is in an open-shell configuration, which are strong candidates to manifest many-body effects. Specifically, we select a linear and a cyclic molecular bridge, i.e., a polyene radical, and a benzene molecule substituted with

a methylene (CH_2) radical group. While both molecules are π -radicals with one electron in the SOMO, we show that many-body effects bring out profound differences. We identify the fingerprint of strong electronic correlations in the splitting of the SOMO resonance. The details of the splitting and the spatial distribution of the SOMO on the molecular backbone have dramatic consequences on the transport properties of the junction.

Finally, we demonstrate that such a splitting cannot be obtained with less sophisticated techniques, such as many-body perturbation theory. We argue that this phenomenon and the underlying microscopic mechanism are general, and apply to a wide family of open-shell molecular systems.

III. METHODS

A. Local orbitals and low-energy models

The LOs method [36] is a transformation-based approach that aims at retrieving hydrogen-like orbitals for atoms in molecules and solids. By construction, LOs are locally orthogonal on each atom. The starting point is a DFT calculation in an AOs basis set. The Hilbert space H is then spanned by a finite set of non-orthogonal orbitals $\{|i\rangle\}$, i.e., with a overlap matrix $\langle i|j\rangle = (\mathbf{S})_{ij} \neq \delta_{ij}$ for $|i\rangle, |j\rangle \in H$. A set of LOs $\{|m\rangle\} \in M \subseteq H$ can be obtained for any atom α in subspace M by a subdiagonalization of the corresponding Hamiltonian sub-block

$$\mathbf{H}_\alpha |m\rangle = \epsilon_m \mathbf{S}_\alpha |m\rangle \quad (1)$$

The LOs are then linear combinations of AOs and are by definition orthogonal on each atom. This allows for a more natural physical interpretation of the LOs as atomic orbitals [36]. In order to obtain an *ab-initio* effective model, we formally separate the Hilbert space into an active space (A) and an environment (E). The active space consists of a subset of LOs $\{|a\rangle\} = A \subseteq M$ which are expected to describe the relevant physics close to the Fermi energy, and at the same time can be efficiently treated within quantum many-body techniques. Instead, the environment consists of all the remaining LOs and AOs, i.e., $\{|e\rangle\} \in E \equiv H \setminus A$. Embedding the active space into the environment ensures that the effective model preserves all information of the original single-particle DFT Hamiltonian [36]. Finally, it is convenient to perform a Löwdin orthogonalization [37] of the LO $\{|a\rangle\}$ states and redefine the A subspace in terms of this new orthonormal basis set with elements

$$|a^\perp\rangle = \sum_a (\mathbf{S}^{-1/2})_{aa^\perp} |a\rangle. \quad (2)$$

Since the overlap between LOs on different atoms is typically low, i.e., $(\mathbf{S})_{ij} \ll 1$, the Löwdin orthonormalization of the active space results only in a weak deformation of the original LOs, which preserves their atomic-like symmetry.

In practice, the LO low-energy model is constructed embedding the active subspace into the environment through a downfolding procedure [38, 39]. Taking into account the non-orthogonality between the A and E subspaces [34], we write the Green's function projected onto the A subspace as

$$\mathbf{G}_A(z) = \mathbf{S}_A^{-1} \mathbf{S}_{AH} \mathbf{G}_H(z) \mathbf{S}_{HA} \mathbf{S}_A^{-1}, \quad (3)$$

where $z = E + i\eta$ is a complex energy with an infinitesimal shift $\eta \rightarrow 0^+$. \mathbf{G}_H denotes the Green's function of the full Hilbert space, and \mathbf{S}_{AH} the overlap matrix between orbitals $|a^\perp\rangle \in A$ and orbitals $|i\rangle \in H$, while the overlap \mathbf{S}_A between the $|a^\perp\rangle$ states is, by construction, the identity matrix and will be omitted in what follows for notational simplicity. The effect of the environment on the A subspace is described by the hybridization function

$$\Delta_A(z) = \mathbf{g}_A^{-1}(z) - \mathbf{G}_A(z)^{-1}, \quad (4)$$

where

$$\mathbf{g}_A = [z - \mathbf{H}_A]^{-1} \quad (5)$$

is Green's function of the isolated A subspace. Rewriting \mathbf{G}_A in terms of Δ_A and using the definition of \mathbf{g}_A yields

$$\mathbf{G}_A(z) = [z - \mathbf{H}_A - \Delta_A(z)]^{-1}. \quad (6)$$

Then, \mathbf{G}_A can be seen as the resolvent of an effective A subspace renormalized by the environment through a dynamical hybridization. The Green's function describes the physics of the whole system, projected onto a subspace.

For a single-particle Hamiltonian, the partition above is arbitrary, and the procedure remains valid independently of the subset of LOs included in the active space. In the context of π -conjugated organic molecules, the projection onto a single p_z LO per C atom (and possibly other species such as N or S) is usually sufficient to achieve a faithful representation of the frontier MOs, and hence suitable to describe the physics close to the Fermi energy [36]. The possibility of considering a restricted subset of LOs in the effective model is of pivotal importance in view of performing computationally-heavy many-body simulations.

B. *cRPA* and *ab-initio* Coulomb parameters

In order to derive the electronic interaction parameters in the A subspace beyond the semi-local density approximations, we employ the constrained Random Phase Approximation (cRPA) [34, 40, 41]. Within the cRPA, we select a region $R \supset A$ where the formation of electron-hole pairs is expected to screen the Coulomb interaction between the A electrons. Because of the strong local nature of the LOs, it is sufficient that R comprises the A

subspace and few atoms nearby. Defining \mathbf{G}_R to be the Green's function projected onto the R subspace in analogy with Eq. (3), the screened Coulomb interaction at the RPA level is given by

$$\mathbf{W}_R = [\mathbf{I} - \mathbf{V}_R \mathbf{P}_R]^{-1} \mathbf{V}_R, \quad (7)$$

where \mathbf{V}_R is the bare Coulomb interaction

$$(\mathbf{V}_R)_{ij,kl} = \int dr \int dr' \psi_i(r) \psi_j^*(r) \frac{e^2}{|r - r'|} \psi_k^*(r') \psi_l(r'), \quad (8)$$

being $\psi_i(r)$ the orbitals in the R region, and \mathbf{P}_R is the static component of the polarizability

$$(\mathbf{P}_R)_{ij,kl} = -2i \int \frac{dz'}{2\pi} \mathbf{G}_{ik}(-z') \mathbf{G}_{lj}(z'). \quad (9)$$

The projection of \mathbf{W}_R onto the A subspace then yields the static screened interaction \mathbf{W}_A . Since we aim at performing many-body simulations of the effective model, we need to partially unscreen the Coulomb parameters, eliminating from \mathbf{W}_A the screening channels arising from A - A transitions included in \mathbf{P}_R , which will be treated at a more sophisticated level of theory. This can be done according to the following prescription

$$\mathbf{U}_A = \mathbf{W}_A [\mathbf{I} + \mathbf{P}_A \mathbf{W}_A]^{-1}, \quad (10)$$

using the polarization \mathbf{P}_A of the A electrons obtained from \mathbf{G}_A similarly to Eq. (9). The matrix elements in \mathbf{U}_A can therefore be regarded as the effective (partially screened) Coulomb parameters.

C. Solutions of the low-energy models

The Green's function of Eq. (6), together with the interactions parameters of Eq. (10), define a low-energy model which can be solved with many-body techniques. Here, we propose two somewhat complementary strategies, i.e., exact diagonalization (ED) and the dynamical mean-field theory (DMFT) [42] as implemented within its real-space generalization (R-DMFT) for inhomogeneous systems [43–47].

1. Exact diagonalization

The ED technique requires a Hamiltonian formulation of the effective model. If the states of the active and embedding subspaces are energetically well-separated, it is possible to neglect the dynamical character of the hybridization function and construct an effective Hamiltonian as

$$\mathbf{H}_A^{\text{eff}} = \mathbf{H}_A + \Delta_A(z=0). \quad (11)$$

Including the screened Coulomb interaction, the model Hamiltonian then reads

$$H = \sum_{ij,\sigma} (\mathbf{H}_A^{\text{eff}} - \mathbf{H}_A^{\text{dc}})_{ij} c_{i\sigma}^\dagger c_{j\sigma} + \frac{1}{2} \sum_{ijkl,\sigma\sigma'} (\mathbf{U}_A)_{ij,kl} c_{j\sigma}^\dagger c_{k\sigma'}^\dagger c_{l\sigma'} c_{i\sigma}, \quad (12)$$

where $c_{i\sigma}^{(\dagger)}$ denote the annihilation (creation) operator of an electron at LO i with spin σ , and the double-counting correction \mathbf{H}_A^{dc} accounts for the interaction already included at the mean-field level by DFT (see Sec. III D). The diagonalization of this Hamiltonian yields the many-body spectrum (eigenstates and eigenvalues) which can be used to construct the Green's function \mathbf{G}_A^{ED} through its Lehmann representation [48]. The many-body self-energy is obtained from the Dyson equation

$$\Sigma_A^{\text{ED}}(z) = z - \mathbf{H}_A^{\text{eff}} - [\mathbf{G}_A^{\text{ED}}(z)]^{-1}, \quad (13)$$

and it describes both local Σ_{ii} and non-local $\Sigma_{i \neq j}$ electronic correlations in the LO basis. An obvious advantage of ED over, e.g., quantum Monte Carlo [49], is that it provides direct access to retarded self-energy and Green's function, and hence the electron transmission function, without the need to perform an analytic continuation numerically, which is an intrinsically ill-defined problem [50]. Note that within ED, we obtain a many-body self-energy which is, by construction, spin-independent, i.e., $\Sigma_{ij}^\sigma = \Sigma_{ij}^{\bar{\sigma}}$ since $\mathbf{H}_A^{\text{eff}}$ follows from a restricted DFT calculation.

2. Real-space DMFT

The idea behind R-DMFT consists of mapping a many-body problem onto a set of auxiliary Anderson impurity models (AIMs) —one for each atom α — described by the projected Green's function [44–46]

$$\mathbf{g}_\alpha^\sigma(z) = (\mathbf{G}_A^\sigma(z))_\alpha. \quad (14)$$

The solution of AIM α (see details below) yields a *local* many-body self-energy $\Sigma_\alpha^\sigma(z)$, so that the self-energy of the A subspace is block diagonal in the atomic subspaces

$$\Sigma_A^\sigma(z) = \text{diag}(\{\Sigma_\alpha^\sigma(z) \mid \alpha \in A\}). \quad (15)$$

The set of auxiliary AIMs are coupled by the Dyson equation

$$\mathbf{G}_A^\sigma(z) = [z + \mu - (\mathbf{H}_A - \mathbf{H}_A^{\text{dc}}) - \Delta_A(z) - \Sigma_A^\sigma(z)]^{-1}, \quad (16)$$

where the Green's function \mathbf{G}_A^σ includes the many-body self-energy and the double-counting correction, and the chemical potential μ is determined to preserve the DFT occupation of the A subspace. Finally, Eqs. (14-16) are iterated self-consistently starting with an initial guess (typically $\Sigma_A^\sigma = 0$) until convergence.

More in detail, in AIM α the impurity electrons interact through a screened local Coulomb repulsion projected onto atom α , i.e., $\mathbf{U}_\alpha = (\mathbf{U}_A)_{ij,kl} \mid i, j, k, l \in \alpha$ [51]. Moreover, the impurity is embedded in a self-consistent *bath* of non-interacting electrons, which describes the rest of the electronic system, encoded in the hybridization function

$$\Delta_\alpha^\sigma(z) = z + \mu - (\mathbf{H}_\alpha - \mathbf{H}_\alpha^{\text{dc}}) - [\mathbf{g}_\alpha^\sigma(z)]^{-1} - \Sigma_\alpha^\sigma(z). \quad (17)$$

Also within R-DMFT, it is convenient to use ED to solve the AIMs to have direct access to retarded functions. This requires to *discretize* the hybridization function with a finite number of bath orbitals, described by orbital energies ϵ_m^σ and hopping parameters to the impurity t_{mi}^σ . The hybridization parameters together with the local Coulomb blocks \mathbf{U}_α , define the AIM Hamiltonian

$$H_{\text{AIM}} = \sum_{ij,\sigma} (\mathbf{H}_\alpha - \mathbf{H}_\alpha^{\text{dc}})_{ij} c_{i\sigma}^\dagger c_{j\sigma} - \mu \sum_{i\sigma} c_{i\sigma}^\dagger c_{i\sigma} + \sum_{m,\sigma} \epsilon_m^\sigma a_{m\sigma}^\dagger a_{m\sigma} + \sum_{mi,\sigma} t_{mi}^\sigma (a_{m\sigma}^\dagger c_{i\sigma} + c_{i\sigma}^\dagger a_{m\sigma}) + \frac{1}{2} \sum_{ijkl,\sigma\sigma'} (\mathbf{U}_\alpha)_{ij,kl} c_{j\sigma}^\dagger c_{k\sigma'}^\dagger c_{l\sigma'} c_{i\sigma}, \quad (18)$$

where $c_{i\sigma}^{(\dagger)}$ and $a_{m\sigma}^{(\dagger)}$ denote the annihilation (creation) operator of an electron at LO i with spin σ , or at bath orbital m with spin σ , respectively. Once the many-body spectrum of the AIM is known, the local self-energy is evaluated in terms of the local Green's function \mathbf{G}_α^σ as

$$\Sigma_\alpha^\sigma(z) = [\mathbf{g}_\alpha^\sigma(z)]^{-1} - [\mathbf{G}_\alpha^\sigma(z)]^{-1}. \quad (19)$$

At convergence, we define the R-DMFT self-energy as

$$\Sigma_A^{\sigma,\text{R-DMFT}}(z) = \Sigma_A^\sigma(z) - \mathbf{H}_A^{\text{dc}} - \mu, \quad (20)$$

so that it contains all shifts related to the density matrix.

In terms of approximations, R-DMFT takes into account local electronic correlations (Σ_{ii}), neglecting non-local correlations (i.e., $\Sigma_{ij} = 0$), but some degree of non-locality is retained as $\Sigma_{ii} \neq \Sigma_{jj}$, and the AIMs are coupled through the self-consistent Dyson equation. Therefore, R-DMFT is suitable to treat intrinsically inhomogeneous systems [26, 46, 47, 52–54]. Moreover, R-DMFT is considerably lighter in terms of computational complexity with respect to the direct ED of the original many-body problem and can treat systems with hundreds of atoms in the active space, inaccessible to ED [26, 44, 46]. Finally, besides the restricted solution $\Sigma_A^\sigma = \Sigma_A^{\bar{\sigma}}$, within R-DMFT we also have the freedom of breaking the spin degeneracy, and describe magnetic solutions [28, 30, 31, 44, 55].

D. Double-counting correction

The double-counting (DC) correction \mathbf{H}_A^{dc} aims at eliminating the correlations in the A subspace included

at a mean-field level by DFT, which are instead to be included in a more sophisticated level of theory within the many-body simulations. Unfortunately, an analytical expression of the correlation effects accounted for within DFT is unknown, and therefore several approximations [47, 56–58] have been developed in the context of DFT+DMFT [59, 60] or DFT+U [61, 62]. For a single-orbital AIM (as in the case of the simulations in this work) the DC correction can be reasonably approximated within the fully localized limit (FFL) [57, 63–65]

$$(\mathbf{H}_A^{\text{dc}})_{ii} = (\mathbf{U}_A)_{ii,ii} \left(n_i^{\text{DFT}} - \frac{1}{2} \right), \quad (21)$$

where n_i^{DFT} is the DFT occupation of orbital i . Hence, we use this form of DC for the R-DMFT calculations. However, there's no established method for the general case of multi-site and multi-orbital Coulomb interaction as is the case for ED. Here, we propose a self-consistent procedure in which a set of local parameters is optimized to fulfill the condition

$$(\mathbf{\Sigma}_A)_{ii}(|z| \rightarrow \infty) = 0, \quad (22)$$

This approach ensures that the electronic properties at high-energies, which are well described by a one-particle approach, are restored to the DFT level.

E. Correlated quantum transport

To describe the electronic transport properties, we use the non-equilibrium Green's function (NEGF) approach [66, 67]. In NEGF, we identify a device region surrounding the nanojunction's constriction and downfold the leads' electrons by virtue of an efficient recursive algorithm [68]. The corresponding Green's function reads

$$\mathbf{G}_D(z) = [z\mathbf{S}_D - \mathbf{H}_D - \mathbf{\Sigma}_L(z) - \mathbf{\Sigma}_R(z) - \mathbf{\Sigma}_D(z)]^{-1}, \quad (23)$$

where $\mathbf{\Sigma}_{L(R)}$ is the self-energy describing the electrons in the left (right) electrodes, and

$$\mathbf{\Sigma}_D(z) = \mathbf{S}_{DA}\mathbf{S}_A^{-1}\mathbf{\Sigma}_A(z)\mathbf{S}_A^{-1}\mathbf{S}_{AD} \quad (24)$$

projects the many-body self-energy of the active space $\mathbf{\Sigma}_A$ (i.e., obtained within either ED or R-DMFT) onto the device region. Following the generalization of the Landauer formula proposed by Meir and Wingreen [69], the conductance is given by

$$G = G_0 T(E_F), \quad (25)$$

where $G_0 = e^2/h$ is the conductance quantum, and the transmission function is computed as

$$T(E) = \text{Tr}[\mathbf{G}_D(z)\mathbf{\Gamma}_L(z)\mathbf{G}_D^\dagger(z)\mathbf{\Gamma}_R(z)], \quad (26)$$

with $\mathbf{\Gamma}_{L(R)}$ the anti-hermitian part of $\mathbf{\Sigma}_{L(R)}$

$$\mathbf{\Gamma}_{L(R)} = i[\mathbf{\Sigma}_{L(R)} - \mathbf{\Sigma}_{L(R)}^\dagger]. \quad (27)$$

While Eqs. (25)–(27) neglect the incoherent contributions (i.e., due to inelastic scattering) to the transmission that arises from the many-body self-energy [35, 70–74], they provide a good approximation of the low-bias transport properties, even in the presence of strong correlations within the A subspace [34, 69].

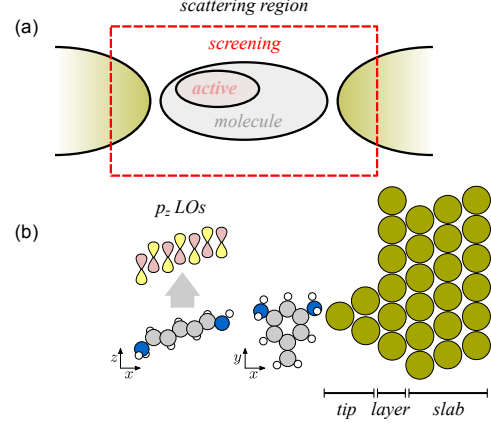


FIG. 1. (a) Schematics of the scattering region of the single-molecule junction, consisting of the molecular bridge and the Au electrodes. The screening region (R) and the active space within the molecule (A) are highlighted. (b) Detailed structure of pentadienyl and benzyl radical, and Au electrodes. For pentadienyl, we also show schematically the mapping onto the C and N p_z LOs.

IV. COMPUTATIONAL DETAILS

The structures were set up with the atomic simulation environment (ASE) software package [75] and the DFT calculations were performed with the GPAW package [76–78]. We performed a geometry optimization, and the atomic positions were relaxed until the forces on each atom were below $0.001 \text{ Hartree/Bohr}^{-1}$ ($\approx 0.05 \text{ eV/\AA}$). For converging the electron density, we used an LCAO double- ζ basis set, with a grid spacing of 0.2 \AA , and the Perdew–Burke–Ernzerhof exchange-correlation functional [79]. For the electron transport calculations, we followed the method described in [68]. The leads were modeled by a three-layer-thick Au(111) slab sampled with a $3 \times 1 \times 1$ k -point grid along the transport direction. The scattering region also includes one Au slab and an additional Au layer terminated by a four-atom Au tip, to which the molecule anchoring groups are attached.

For all structures, the A subspace describing the effective model is composed of the p_z LOs of the C and N atoms of the molecular bridge, while the R subspace for the cRPA calculation of the screened interaction includes the molecule and also extends to the Au atoms of the tip (see Fig. 1).

V. INIGHTS FROM AB-INITIO SIMULATIONS

In order to understand the many-body effects arising in the open-shell configuration, it is useful to recall some chemical and electronic properties of the pentadienyl and benzyl radicals, and how those are reflected by *ab-initio* simulations. In particular, we look at the spatial distribution of the SOMO and at the *ab-initio* Coulomb parameters projected onto the LOs of the active space.

A. Structure of the SOMO

The pentadienyl radical (C_5H_7) is a linear molecule, and the shortest polyene radical after allyl. It has three resonant structures. In each structure, the unpaired electron is hosted on one of the *odd* C atoms. The delocalization of the unpaired electron along the molecular backbone contributes to the thermodynamical stability of the molecule [80, 81]. The structure we consider is obtained by substituting a hydrogen atom at each end of the chain by an amino group. By diagonalization of the AOs Hamiltonian in the subspace of the molecule, we find an eigenvalue just above the Fermi energy, corresponding to a partially occupied MO (i.e., the SOMO). The pentadienyl resonant structures and the projection of the SOMO onto the p_z LOs of the active space are shown in Figs. 2(a,b), respectively. The SOMO reflects the resonant structures, with the largest projection on the odd- and nodes at even- C atoms. It also displays a significant projection onto the anchoring groups, suggesting a strong coupling to the electrodes in the junction.

The benzene molecule (C_6H_6) is a cyclic aromatic hydrocarbon and the archetypical building block for molecular electronics. For our analysis, we consider a related compound, the benzyl radical ($C_6H_5CH_2^\cdot$), which is obtained by substituting a hydrogen atom with a methylene (CH_2) group. The benzyl radical is also stabilized by resonance but, unlike pentadienyl, in both resonant structures the unpaired electron is hosted on the benzylic C, as illustrated in Fig. 2(c). We focus on the *meta* configuration, in which the amino groups are substituted at the 1,3-positions of the aromatic ring, while the methylene group is substituted in the 5-position, i.e., along the longer branch of the ring (see also Fig. 1). As expected, we find an eigenvalue lying at the Fermi energy, corresponding to the SOMO shown in Fig. 2(d). The SOMO displays the largest projection at the p_z LO of the benzylic C atom and displays nodes at every other C (similarly to pentadienyl). However, it does not extend to the anchoring groups, thus suggesting a weak coupling to the electrodes.

B. Coulomb parameters in the LO basis

The partially screened Coulomb matrix projected onto the LO basis of the active space $U_{ij} = (U_A)_{ij}$ is shown in

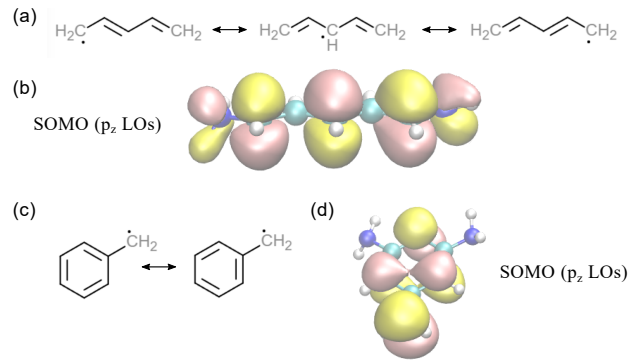


FIG. 2. Resonances and SOMO isosurface (from LOs p_z) of pentadienyl (a,b) and benzyl (c,d) radicals. In pentadienyl, the unpaired electron is hosted by one of the *odd* C of the polyene chain, which also display the largest contributions in the isosurface, while the *even* C correspond to nodes. In both benzyl resonant structures, the unpaired electron is hosted by the benzylic C, and the isosurface displays nodes on every other C, similarly as in pentadienyl. Isovalues: ± 0.03 au.

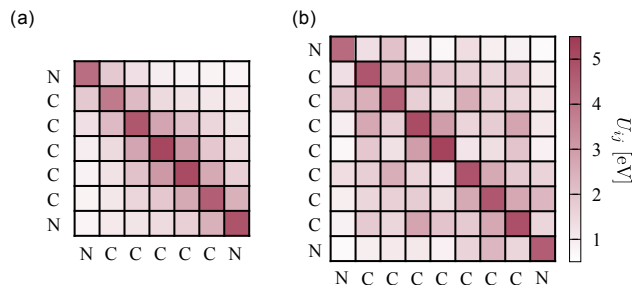


FIG. 3. Partially screened Coulomb parameters $U_{ij} = (U_A)_{ij}$ in the LO basis for the pentadienyl (a) and the benzyl (b) radicals.

Figs. 3(a,b) for the pentadienyl and the benzyl radicals, respectively. In both cases, the intra-orbital couplings U_{ii} are in the range of 4–5 eV and are slightly stronger for the atoms farther away from the metallic Au electrodes, due to the weaker screening effects. Similar values of the Coulomb repulsion are found for the anchoring groups. However, as we shall see later, while the Cp_z LOs are close to half-filling the Np_z LOs are almost full, resulting in weak correlation effects.

VI. ELECTRON TRANSPORT

We start our analysis by looking at the electron transport properties of the pentadienyl and benzyl junctions. In particular, we compare the predictions of DFT and many-body simulations, where the Coulomb repulsion is treated at different levels of approximation.

A. Pentadienyl

Within DFT, the transmission function displays a resonance close to the Fermi energy (denoted by E_F) corresponding to ballistic transport through the SOMO. The resonance is found at $\epsilon_{\text{SOMO}} = 70$ meV and has a width $\Gamma_{\text{SOMO}} \approx 300$ meV, reflecting a significant hybridization of the SOMO with the states of the electrodes. The slight misalignment between the SOMO resonance and E_F , yield a conductance $G = 5.7 \times 10^{-1} G_0$ in each spin channel, see Fig. 4(a). This scenario changes as the SOMO resonance is split due to the Coulomb repulsion. However, depending on the splitting mechanism, we observe fundamentally different transport properties.

Within spin-unrestricted R-DMFT calculations, the spin rotational symmetry is broken. The doublet degeneracy is lifted as the SOMO is split into an occupied state in the majority-spin channel (e.g., \downarrow -SOMO) and an unoccupied state in the minority-spin channel (\uparrow -SUMO). This approximation yields a magnetic insulator with a spin gap $\Delta_s \approx 1.3$ eV and a magnetic moment $\langle S_z \rangle \simeq 1/2$ due to the single unpaired electron. The spin-dependent splitting of a transmission feature, e.g., a resonance [16, 17, 82] or an antiresonance [30, 31], has been suggested as a suitable mechanism for the realization of organic spin filters. For pentadienyl, the splitting is approximately symmetric around the Fermi level, thus yielding a similar conductance in the two spin channels $G^\uparrow = 1.9 \times 10^{-2} G_0$ and $G^\downarrow = 1.5 \times 10^{-2} G_0$ and low spin-filtering efficiency. The spin-unrestricted R-DMFT transmission functions are shown in Fig. 4(a).

Another possible mechanism to split the SOMO is obtained *without* lifting the spin degeneracy (i.e., within

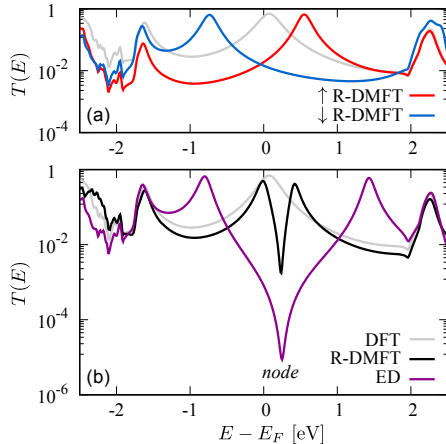


FIG. 4. Electron transmission function through the pentadienyl radical junction. DFT predicts a SOMO resonance close to E_F . Taking into account the Coulomb repulsion beyond restricted DFT yields: (a) a splitting of the resonance into \downarrow -SOMO and \uparrow -SUMO due to spin-symmetry breaking; (b) a splitting of the resonance without symmetry breaking and a transmission node due to many-body effects.

either R-DMFT or ED). In this case, we find that the SOMO transmission resonance is split, revealing an underlying transmission node, see Fig. 4(b). Hence, many-body calculations predict a strong suppression of the conductance, by several order of magnitude, in stark contrast with the single-particle picture, in which electron transport is dominated by a nearly-resonant ballistic channel. Note that the splitting is substantially larger in ED than in R-DMFT, and considering that the antiresonance is not aligned with E_F , it also results in a much stronger suppression of the conductance $G = 8.1 \times 10^{-4} G_0$ (ED) versus $G = 4.9 \times 10^{-1} G_0$ (R-DMFT). This suggests that non-local effects play an important role, as it can be expected in low-dimensional systems [27, 32].

Since a linear π -conjugated molecule does not display any topological node, the pentadienyl node has been suggested to arise from destructive interference between different charged states of the molecule [14]. In Sec. VII, we discuss in detail the microscopic mechanism responsible for the splitting of the SOMO and for the transmission node, and show that they are intertwined.

B. Benzyl

In the case of benzene single-molecule junctions, there is more than one possible configuration for the ring to bridge the electrodes, depending on the position of the amino anchoring groups. We focus on the *meta* configuration (i.e., amino groups substituted at the 1,3-positions of the aromatic ring) which is particularly relevant in the context of molecular electronics.

Within DFT, the transmission function displays two striking features which can be readily identified in Figs. 5(a,b): a narrow asymmetric Fano resonance at $\epsilon_{\text{Fano}} < 10$ meV, close to E_F , and a wide antiresonance at $\epsilon_{\text{DQI}} \approx -0.8$ eV. Both features originate from quantum interference (QI) effects. Clarifying the nature of the resonances and highlighting their differences, will prove helpful in understanding how electronic correlations affect the transport properties and to shed light on the underlying microscopic mechanism.

The Fano resonance has a characteristic asymmetric line shape and arises from the QI between the SOMO, which is mostly localized at the benzylic C atom, and the delocalized MOs on the molecular backbone, which have a strong overlap with the states of the metallic Au electrodes [83–85]. The antiresonance is the hallmark of destructive QI in the meta configuration and it is well-established in the literature, from both the experimental [86–88] and theoretical [89–93] points of view. It arises from the interference between the HOMO and LUMO of the ring itself [93]. There is a subtle interplay between the antiresonance and the functional groups (not necessarily radical). It is well-established that substituents and adsorbates affect the relative position of destructive interference features with respect to the Fermi energy. The chemical control of the antiresonance can be exploited

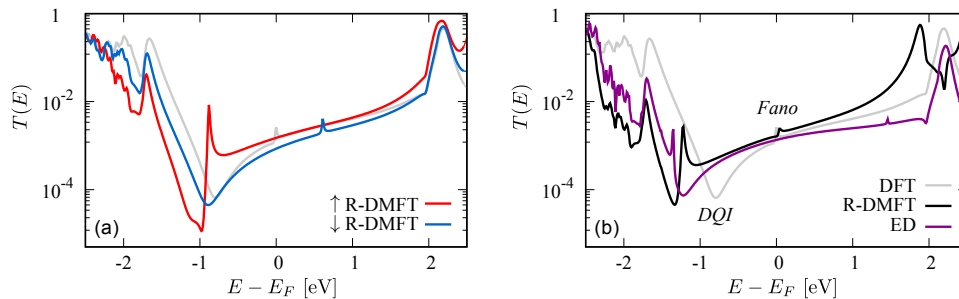


FIG. 5. Electron transmission function through the benzyl radical junction, displaying the Fano and antiresonance originating by quantum interference effects. (a) Breaking the spin symmetry results in the spin-splitting of both the Fano and the DQI features. (b) Including many-body effects beyond DFT, the Fano resonance is split (without symmetry-breaking) while the DQI antiresonance is shifted to lower energies.

for a wide range of applications ranging from nanoelectronics [94] to chemical sensing [95, 96]. In principle, the position of the antiresonance is also influenced by the substitution position in the ring (see, e.g., [94] and references therein), but this effect is of marginal relevance to the scope of the present work.

The Fano resonance is indeed the transport signature of the SOMO. However, in contrast to pentadienyl, where the SOMO is delocalized along the molecular backbone and dominates the electron transport, in benzyl, the SOMO is mostly localized on the methyl functional group. It is therefore interesting to investigate the effect of the Coulomb repulsion and highlight the differences between the two cases. Within restricted DFT simulations, the narrow Fano resonance is partially concealed by the wider QI antiresonance. Breaking the spin symmetry within spin-unrestricted R-DMFT yields a pair of spin-split Fano resonances, as shown in Fig. 5(a). In the majority spin channel, $\epsilon_{\text{Fano}}^{\uparrow} < 0$ falls within the transmission depletion caused by the antiresonance and the asymmetric Fano profile is clearly observable. Its counterpart in the minority spin channel is found above E_F , i.e., $\epsilon_{\text{Fano}}^{\downarrow} > 0$, and is still mostly concealed by the background transmission. Interestingly, the spin-symmetry breaking also induces spin-resolved QI antiresonances [30, 31, 97] but the splitting $\epsilon_{\text{DQI}}^{\downarrow} - \epsilon_{\text{DQI}}^{\uparrow}$ is however weaker than in the Fano case, since the spin imbalance yields $\langle S_z \rangle \simeq 1/2$ on the p_z LO of the benzylic C, and a weaker magnetization in the rest of the molecule.

Not allowing breaking the spin symmetry in the many-body simulations reveal another scenario, as shown in Fig. 5(b). The difference is twofold. We observe a splitting of the Fano resonance in both R-DMFT and ED (with the ED splitting being significantly larger) but no splitting is detected for the QI antiresonance, which is rather shifted further away from E_F . This suggests that the microscopic mechanism behind the splitting with and without spin-symmetry breaking are fundamentally different, as it distinguishes between the two QI features. Moreover, in contrast to the case of pentadienyl, the splitting of the SOMO in benzyl does not result in a strong

suppression of the transmission within the SOMO-SUMO gap. The two observations above are deeply connected, and eventually, they can both be rationalized in terms of the spatial distribution of the SOMO.

VII. MICROSCOPIC MECHANISM

A. Splitting of the SOMO

So far, we have seen that the Coulomb repulsion induces a splitting of the SOMO of the organic radicals. In order to gain a deeper understanding of the electronic mechanism behind the splitting, and how it affects the transport properties of the junction, it is useful to look at the retarded self-energy in the LO basis $\Sigma_{ij} = (\Sigma_A)_{ij}$, corresponding to Σ_A^{ED} and $\Sigma_A^{\sigma, \text{R-DMFT}}$ in Eqs. (13, 20), respectively. The many-body effects encoded in the self-energy can be rationalized by interpreting the real part as an energy-dependent level shift, and the imaginary part as an effective electron-electron scattering rate. We argue that the mechanism discussed in the following is a common feature of organic radicals. Therefore, we discuss the pentadienyl and benzyl radicals in parallel and highlight the differences whenever necessary.

In order to compare the different approximations, it is convenient to look at the trace of the self-energy matrix. Within spin-unrestricted R-DMFT, which is shown in Figs. 6(a,d), the real part of the self-energy is weakly energy-dependent around E_F , and determines a shift of the SOMO resonance in opposite directions for the two spin polarizations. The imaginary part is negligible (not shown) resulting in highly coherent SOMO and SUMO electronic excitations below and above E_F . Note that the ground state of spin-unrestricted R-DMFT is two-fold degenerate, and it is invariant under a flip of all spins: $\{\sigma_i\} \rightarrow \{\bar{\sigma}_i\}$. This picture is qualitatively analogous to what one can expect also at the single-particle level, i.e., within DFT+U. Many-body effects are weak, and the dominant effect arises from the spin-symmetry breaking, as both radicals are magnetic insulators with a

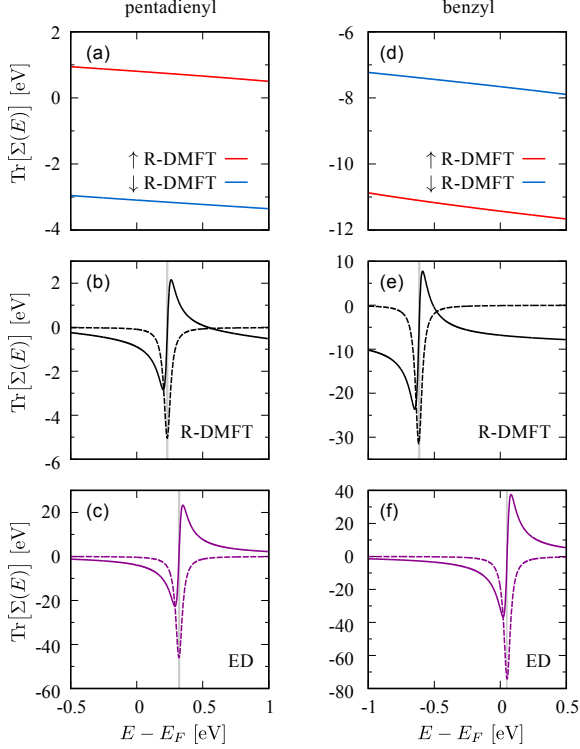


FIG. 6. Trace of the retarded self-energy $\text{Tr}[\Sigma(E)]$ in the LO basis for the pentadienyl (a,b,c) and benzyl (d,e,f) radicals (the real and imaginary parts are denoted by solid and dashed lines, respectively). Within spin-unrestricted R-DMFT (a,d) the self-energy displays a weakly energy-dependent real part, which is different in each spin sector, while the imaginary part is negligible (not shown). Within both R-DMFT (b,e) and ED (c,f) the self-energy is dominated by a single resonance at energy ϵ_r (denoted by a solid grey line).

spin SOMO-SUMO gap.

The scenario is completely different within restricted R-DMFT and ED, as shown in Figs. 6(b,c,e,f). There, the self-energy is dominated by a single resonance and its energy dependence can be well described within a one-pole approximation (OPA)

$$\Sigma_{\text{OPA}}(E) = \frac{a}{E - E_F - \epsilon_r + i\gamma}. \quad (28)$$

The OPA self-energy has a Lorentzian shape, where ϵ_r and γ denote the resonant energy and the width of the resonance, whereas a controls the amplitude of the curve. The imaginary part of the self-energy plays the role of a *giant* electron-electron scattering rate and suppresses electronic excitations around $\epsilon_r \simeq \epsilon_{\text{SOMO}}$, while the real part redistributes the spectral weight towards higher energies. This many-body mechanism, akin to the Mott metal-to-insulator transition as described within DMFT [42], is at the origin of the splitting of the SOMO resonance.

In organic radicals, the following hierarchy of emergent energy scales is realized: $\Gamma_{\text{SOMO}} \ll \Delta \lesssim U_{\text{screened}}$, where

the typical energy scale associated with the screened Coulomb repulsion U_{screened} significantly exceeds the narrow width of the SOMO resonance ($\sim 10\text{--}100$ meV), and the HOMO-LUMO single-particle gap Δ controlled by the C-C π -bonds (\sim eV). This sets the electrons in the SOMO deep within the strongly correlated regime. Such a general condition suggests this mechanism to be common to organic radicals with a single unpaired electron. Multi-radical molecules [98] and networks [99], may display different electronic and transport properties due to effective interactions between the unpaired electrons [7, 18–20].

B. Spatial structure of the electronic correlations

While R-DMFT and ED seem to qualitatively describe the same many-body mechanism for the splitting of the SOMO, it is also interesting to look at the whole self-energy matrix. As discussed in Sec. III C, within ED all elements $\Sigma_{ij} \neq 0$, whereas within R-DMFT $\Sigma_{ij} \propto \delta_{ij}$. Remarkably, all elements of the self-energy (irrespective of the approximation) are well described by the OPA with the *same* resonant energy ϵ_r , as shown in Figs. 7(a,e). The off-diagonal elements (when non-zero) can have either sign since it is not determined by causality. It is then easy to have a comprehensive look at the self-energy by plotting the matrix $\Sigma_{ij}(\epsilon_r)$, as shown in Figs. 7(c,d,g,h).

Indeed, looking at the ED self-energy matrix, clear patterns emerge. Along the diagonal, some elements Σ_{ii} are significantly larger than the others (note the logarithmic scale), and this asymmetry is mirrored by the off-diagonal elements. Upon close inspection, we can associate them with the p_z LOs with the largest SOMO projection, thus confirming that the strongest many-body effects correlate with the spatial distribution of the SOMO. Within R-DMFT, we find an analogous pattern along the diagonal, as indicated in the insets.

Despite its approximations (local Coulomb interaction, local correlations), it seems that R-DMFT tells qualitatively the same story as the full ED simulations. This advocates for a substantially local character of the microscopic mechanism, that can describe both the splitting of the SOMO and its consequences on electron transport, whereas non-local effects renormalize the splitting.

C. Implications for electron transport

The many-body mechanism behind the splitting of the SOMO is common to both the pentadienyl and benzyl radicals. However, its consequences on electron transport are dramatically different. In order to understand why, it is necessary to combine the insights from DFT with the knowledge about the spatial and energy structure of the self-energy.

In pentadienyl, the SOMO is delocalized throughout the molecular backbone, and its large projection on the

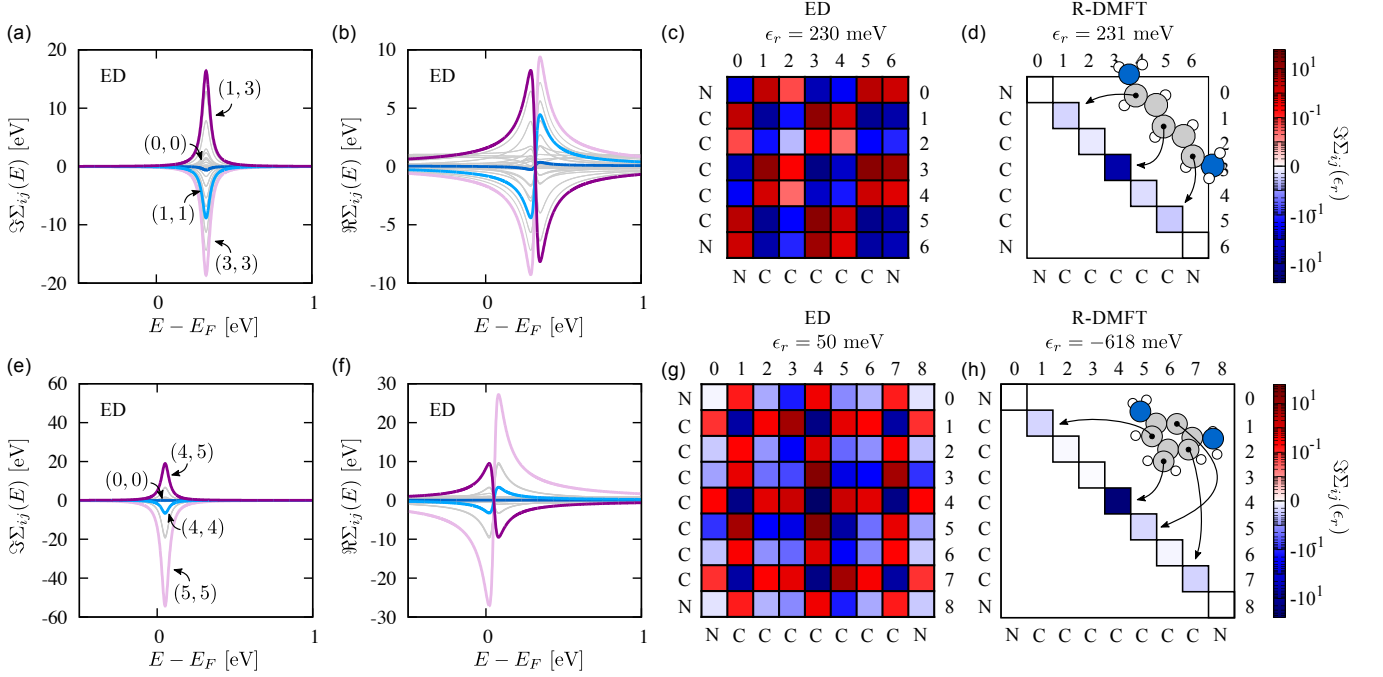


FIG. 7. Component of the ED self-energy $\Sigma_{ij}(E)$ and its matrix representation at the resonant energy $\text{Im} \Sigma_{ij}(\epsilon_r)$ in the LO basis for the pentadienyl (a,b,c,d) and benzyl (e,f,g,h) radicals. Each component of the self-energy (grey lines) is dominated by a single pole (a,b,e,f) at a resonant energy ϵ_r . Selected components (i, j) are highlighted (color lines) and are labeled according to their index in the matrix. The matrix structure of the self-energy reflects the spatial distribution of the SOMO, i.e., the largest local (Σ_{ii}) and non-local ($\Sigma_{ij \neq i}$) self-energy contributions are found for the LOs with the largest projections to the SOMO (denoted by arrows, see also Fig. 2). Within R-DMFT (d,h) the self-energy is diagonal in the LO indices $\Sigma_{ij} \propto \delta_{ij}$ and displays the same pattern.

p_z LOs of the anchoring groups (see Fig.2(a)) ensures a substantial overlap with the states in the metallic electrodes. Hence, there is a transmission channel across the junction through the SOMO. The pole of the self-energy results in a zero of the corresponding Green's function. The suppression of the Green's function hinders electron transport at that energy and is at the origin of the transmission node [30, 31]. In contrast, in the benzyl radical, the SOMO has negligible projection on the amino groups (see Fig.2(d)) and transport is dominated by transmission channels involving the frontier MOs. Therefore, the splitting of the Fano resonance weakly affects those channels, and does not prevent the off-resonance transmission of electrons across the junction.

The above picture can be essentially reproduced within the following tight-binding (TB) three-orbital model, which is schematically represented in Fig. 8(a). Let us consider three orbitals (ℓ, c, r) that can be interpreted as the amino groups, left (ℓ) and right (r), and the central molecule (c). The Hamiltonian in such a basis reads

$$\mathbf{H} = \begin{pmatrix} \epsilon_\ell & t & t' \\ t & \epsilon_c & t \\ t' & t & \epsilon_r \end{pmatrix}. \quad (29)$$

The hybridization to the electrodes is mediated by the external (ℓ, r) orbitals and, for the sake of this discussion,

it is assumed to be energy-independent:

$$\mathbf{\Gamma}_L = \begin{pmatrix} \Gamma & 0 & 0 \\ 0 & 0 & 0 \\ 0 & 0 & 0 \end{pmatrix}, \quad \mathbf{\Gamma}_R = \begin{pmatrix} 0 & 0 & 0 \\ 0 & 0 & 0 \\ 0 & 0 & \Gamma \end{pmatrix}. \quad (30)$$

The Hamiltonian of the isolated system can be diagonalized to obtain the eigenvalues ϵ_{HOMO} , ϵ_{SOMO} , and ϵ_{LUMO} . In light of the results shown in Fig. 7, the Green's function of the device

$$\mathbf{G}_D(z) = [z - \mathbf{H} + i\mathbf{\Gamma}_L/2 + i\mathbf{\Gamma}_R/2 - \mathbf{\Sigma}_D(z)]^{-1} \quad (31)$$

is dressed with an OPA self-energy

$$\mathbf{\Sigma}_D(z) = \begin{pmatrix} 0 & 0 & 0 \\ 0 & \Sigma_{\text{OPA}}(z) & 0 \\ 0 & 0 & 0 \end{pmatrix} \quad (32)$$

which acts on the central part (see Fig. 7(a,e) for a connection with the *ab-initio* simulations) and has a pole at ϵ_{SOMO} . Within such a three-orbital model, the Landauer transmission in Eq. (26) simplifies to

$$T(E) = \Gamma^2 |G_{\ell r}(E)|^2, \quad (33)$$

where $G_{\ell r} = (\mathbf{G}_D)_{\ell r}$ is the upper-right element of the Green's function, linking the orbitals connected to the

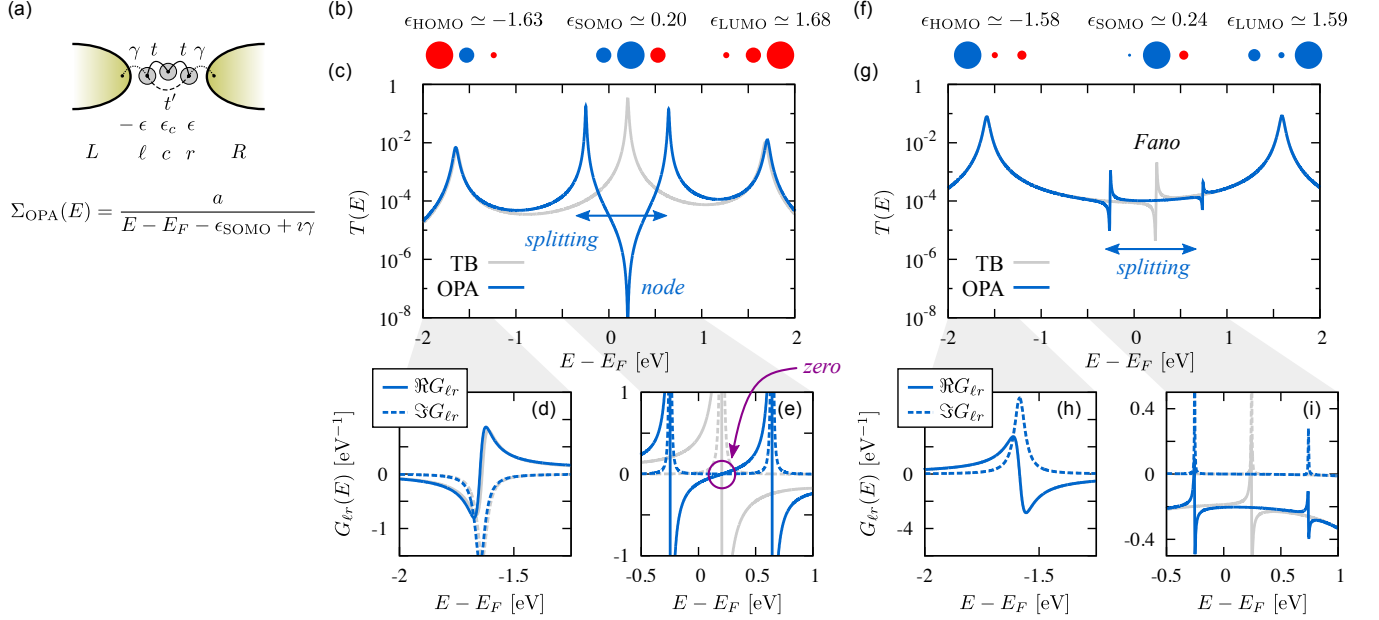


FIG. 8. Schematic representation of the three-orbital TB model with its parameter, and form of the OPA self-energy (a). Weight distribution and eigenvalues of the TB MOs for scenarios representative of the pentadienyl (b) and benzyl (f) radicals. The transmission function (c,g) obtained without (grey lines) and with (blue lines) the OPA self-energy captures all relevant features of the DFT and many-body simulations. The Green's function $G_{\ell r}$ is shown for specific energy ranges, which are relevant to explaining the spectral features associated with the HOMOs (d,h) and the SOMOs (e,i), as discussed in the text. Model parameters [eV]: $\epsilon = 0.5$, $\epsilon_c = 0.25$, $a = 0.25$, $\Gamma = 0.05$, $\gamma = 0.003$, common to both scenarios, $t = 0.5$, $t' = 0$ (b,c,d) and $t = 0.1$, $t' = 0.5$ (e,f,g).

electrodes, and describes the only transmission channel across the junction.

For the sake of simplicity, one can take $-\epsilon_\ell = \epsilon_r = \epsilon$, and $\epsilon_c \ll \epsilon$, which together with a , Γ , and η are kept fixed, whereas we choose the parameters t and t' to describe two scenarios, which are representative of the pentadienyl and benzyl radicals. The results are shown in Fig. 8 and described in the following.

The physics of the pentadienyl radical can be reproduced by choosing $t \lesssim \epsilon$ and $t' = 0$. The corresponding TB MOs are fairly delocalized throughout the system, as shown in Fig. 8(b). Hence, electron transport happens through sequential hopping processes through the c orbital. The transmission function, Fig. 8(c), displays a SOMO resonance which is split by including the OPA self-energy, revealing a transmission node within the SOMO-SUMO gap. The origin of the transmission node is ascribed to a zero of the Green's function at the SOMO energy $G_{\ell r}(E \simeq \epsilon_{\text{SOMO}})$ [30, 31] as demonstrated in Fig. 8(e).

Instead, with the choice of parameters $t \ll t' \lesssim \epsilon$, one can describe the physics of the benzyl radical, characterized by an orbital c , which is weakly coupled to the $\ell - r$ molecular backbone. The corresponding SOMO is fairly localized on the central orbital, see Fig. 8(f). The transmission function displays a Fano resonance which is split by the OPA self-energy see Fig. 8(g). In contrast to the previous case, $G_{\ell r}$ does not have a zero, and trans-

port is dominated by a transmission channel that bridges the electrodes through the direct $\ell - r$ hopping t' . Finally, note that in both scenarios above, many-body effects are negligible for the HOMO and LUMO resonances (corresponding to states which are completely filled and empty, respectively) even when the ‘‘correlated’’ c orbital has a sizable hybridization with ℓ and r , cfr. Figs. 8(c,d,g,h).

Hence, the three-orbital model can reproduce all fundamental features of the radical junctions discussed in this work, and at the same time, provides a simple interpretation of the numerical simulations.

D. Non-perturbative nature of the splitting

Within ED and R-DMFT, the solution of the many-body problem (i.e., on the lattice or the auxiliary AIM) is *numerically exact*. This means that the Coulomb repulsion is taken into account in a *non-perturbative* way. It is interesting to compare these results to a *perturbative* approach, e.g., within the *GW* approximation [100, 101], which has been extensively and successfully applied to molecules [102–107]. However, the question arises to which extent many-body perturbation theory approaches are able to describe the physics of open-shell systems [108]. Within *GW*, the self-energy is computed to the lowest order in perturbation theory, as a convolution of the Green's function and the screened in-

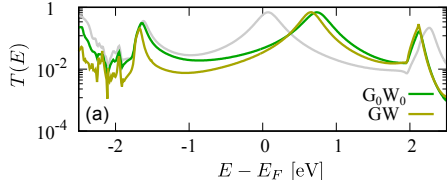


FIG. 9. Electron transmission function through the pentadienyl radical junction. Both the G_0W_0 and the self-consistent GW approximations fail to predict the splitting of the SOMO, as described within ED and R-DMFT, cfr. Fig 4.

teraction. We compute the GW self-energy correction projected onto the A region

$$\Sigma(z) = \mathbf{G}_A(z)\mathbf{W}_A, \quad (34)$$

as described in [68], and we consider the case of the pentadienyl radical without loss of generality.

In Fig. 9 we see that neither G_0W_0 nor the fully self-consistent GW approximation is able to induce a splitting of the SOMO resonance, and the numerical simulations rather result in a shift of the corresponding resonance above the Fermi energy. Hence, the many-body techniques we propose to investigate open-shell molecules are not only *sufficient* but also *necessary* for our goal, whereas less sophisticated approaches fall short in describing the electronic and transport properties arising from the strong electronic correlations within the SOMO.

VIII. CONCLUSIONS

In this work, we have proposed a numerical method that combines *ab-initio* with state-of-the-art many-body techniques and is able to address the complexity of a realistic chemical environment as well as electronic correlation effects beyond the single-particle picture. The deliverable of this project served to shed light on the mechanism governing the electronic and transport properties of quantum junctions with organic molecules in an open-shell configuration. By considering a linear and a cyclic radical molecule, we derive a general understanding of the role of many-body effects in molecular radicals with a single unpaired electron, and we show that they have dramatic consequences on electron transport. We establish the microscopic mechanism behind the splitting of the SOMO resonance and unravel a clear link between the space-time structure of electron-electron correlations and the spatial distribution of the SOMO. We demonstrate this by proposing a minimal model, which is capable of grasping the microscopic mechanism and thus reproducing all relevant features of the transmission properties. Our work will pave the path toward a deeper and more comprehensive understanding of strongly correlated electron physics at the nanoscale.

ACKNOWLEDGEMENTS

We thank J. M. Tomczak for valuable discussions. This research is supported by the Austrian Science Fund (FWF) through project P 31631 (A.V., R.S.) and by the NCCR MARVEL funded by the Swiss National Science Foundation grant 51NF40-205602 (G.G., D.P., M.L.). Computational support from the Swiss Supercomputing Center (CSCS) under project ID s1119 is gratefully acknowledged.

-
- [1] S. Sanvito, Chemical Society Reviews **40**, 3336 (2011), URL <https://doi.org/10.1039/c1cs15047b>.
 - [2] W. Zeng and J. Wu, Chem **7**, 358 (2021), URL <https://doi.org/10.1016/j.chempr.2020.10.009>.
 - [3] Z. Chen, Y. Li, and F. Huang, Chem **7**, 288 (2021), URL <https://doi.org/10.1016/j.chempr.2020.09.024>.
 - [4] R. Frisenda, R. Gaudenzi, C. Franco, M. Mas-Torrent, C. Rovira, J. Veciana, I. Alcon, S. T. Bromley, E. Burzuri, and H. S. J. van der Zant, Nano Letters **15**, 3109 (2015), URL <https://doi.org/10.1021/acs.nanolett.5b00155>.
 - [5] F. Bejarano, I. J. Olavarria-Contreras, A. Droghetti, I. Rungger, A. Rudnev, D. Gutiérrez, M. Mas-Torrent, J. Veciana, H. S. J. van der Zant, C. Rovira, et al., Journal of the American Chemical Society **140**, 1691 (2018), URL <https://doi.org/10.1021/jacs.7b10019>.
 - [6] L. L. Patera, S. Sokolov, J. Z. Low, L. M. Campos, L. Venkataraman, and J. Repp, Angewandte Chemie International Edition **58**, 11063 (2019), URL <https://doi.org/10.1002/anie.201904851>.
 - [7] Y. Zheng, C. Li, C. Xu, D. Beyer, X. Yue, Y. Zhao, G. Wang, D. Guan, Y. Li, H. Zheng, et al., Nature Communications **11** (2020), URL <https://doi.org/10.1038/s41467-020-19834-2>.
 - [8] J. Liu, H. Isshiki, K. Katoh, T. Morita, K. B. Brian, M. Yamashita, and T. Komeda, Journal of the American Chemical Society **135**, 651 (2012), URL <https://doi.org/10.1021/ja303510g>.
 - [9] Y. hui Zhang, S. Kahle, T. Herden, C. Stroh, M. Mayor, U. Schlickum, M. Ternes, P. Wahl, and K. Kern, Nature Communications **4** (2013), URL <https://doi.org/10.1038/ncomms3110>.
 - [10] R. Requist, S. Modesti, P. P. Baruselli, A. Smogunov, M. Fabrizio, and E. Tosatti, Proceedings of the National Academy of Sciences **111**, 69 (2013), URL <https://doi.org/10.1073/pnas.1322239111>.
 - [11] A. Droghetti and I. Rungger, Physical Review B **95** (2017), URL <https://doi.org/10.1103/physrevb.95.085131>.

- [12] W. H. Appelt, A. Droghetti, L. Chioncel, M. M. Radonjić, E. Muñoz, S. Kirchner, D. Vollhardt, and I. Rungger, *Nanoscale* **10**, 17738 (2018), URL <https://doi.org/10.1039/c8nr03991g>.
- [13] Y. Ji, L. Long, and Y. Zheng, *Materials Chemistry Frontiers* **4**, 3433 (2020), URL <https://doi.org/10.1039/d0qm00122h>.
- [14] J. P. Bergfield, G. C. Solomon, C. A. Stafford, and M. A. Ratner, *Nano Letters* **11**, 2759 (2011), URL <https://doi.org/10.1021/nl201042m>.
- [15] D. Hernangómez-Pérez, S. Gunasekaran, L. Venkataraman, and F. Evers, *Nano Letters* **20**, 2615 (2020), URL <https://doi.org/10.1021/acs.nanolett.0c00136>.
- [16] M. Smeu and G. A. DiLabio, *The Journal of Physical Chemistry C* **114**, 17874 (2010), URL <https://doi.org/10.1021/jp105589y>.
- [17] C. Herrmann, G. C. Solomon, and M. A. Ratner, *Journal of the American Chemical Society* **132**, 3682 (2010), URL <https://doi.org/10.1021/ja910483b>.
- [18] S. Mishra, G. Catarina, F. Wu, R. Ortiz, D. Jacob, K. Eimre, J. Ma, C. A. Pignedoli, X. Feng, P. Ruffieux, et al., *Nature* **598**, 287 (2021).
- [19] E. Turco, S. Mishra, J. Melidonie, K. Eimre, S. Obermann, C. A. Pignedoli, R. Fasel, X. Feng, and P. Ruffieux, *The journal of physical chemistry letters* **12**, 8314 (2021).
- [20] D. Jacob and J. Fernández-Rossier, *Physical Review B* **106**, 205405 (2022).
- [21] S. Bhandary, J. M. Tomczak, and A. Valli, *Nanoscale Advances* **3**, 4990 (2021), URL <https://doi.org/10.1039/d1na00407g>.
- [22] F. Gao, R. E. Menchón, A. Garcia-Lekue, and M. Brandbyge, *Tunable spin and transport in porphyrin-graphene nanoribbon hybrids* (2022), URL <https://arxiv.org/abs/2210.13610>.
- [23] J. P. Perdew, *International Journal of Quantum Chemistry* **28**, 497 (2009), URL <https://doi.org/10.1002/qua.560280846>.
- [24] M. Sentef, J. Kuneš, P. Werner, and A. P. Kampf, *Phys. Rev. B* **80**, 155116 (2009), URL <https://link.aps.org/doi/10.1103/PhysRevB.80.155116>.
- [25] F. Hüsler, T. Olsen, and K. S. Thygesen, *Physical Review B* **87** (2013), URL <https://doi.org/10.1103/physrevb.87.235132>.
- [26] A. Valli, G. Sangiovanni, A. Toschi, and K. Held, *Physical Review B* **86**, 115418 (2012).
- [27] A. Valli, T. Schäfer, P. Thunström, G. Rohringer, S. Andergassen, G. Sangiovanni, K. Held, and A. Toschi, *Physical Review B* **91** (2015), URL <https://doi.org/10.1103/physrevb.91.115115>.
- [28] A. Valli, A. Amaricci, A. Toschi, T. Saha-Dasgupta, K. Held, and M. Capone, *Physical Review B* **94** (2016), URL <https://doi.org/10.1103/physrevb.94.245146>.
- [29] M. Schüler, S. Barthel, T. Wehling, M. Karolak, A. Valli, and G. Sangiovanni, *The European Physical Journal Special Topics* **226**, 2615 (2017), URL <https://doi.org/10.1140/epjst/e2017-70049-3>.
- [30] A. Valli, A. Amaricci, V. Brosco, and M. Capone, *Nano Letters* **18**, 2158 (2018), URL <https://doi.org/10.1021/acs.nanolett.8b00453>.
- [31] A. Valli, A. Amaricci, V. Brosco, and M. Capone, *Physical Review B* **100** (2019), URL <https://doi.org/10.1103/physrevb.100.075118>.
- [32] P. Pudleiner, P. Thunström, A. Valli, A. Kauch, G. Li, and K. Held, *Physical Review B* **99** (2019), URL <https://doi.org/10.1103/physrevb.99.125111>.
- [33] A. I. Krylov, in *Reviews in Computational Chemistry* (John Wiley & Sons, Inc., 2017), pp. 151–224, URL <https://doi.org/10.1002/9781119356059.ch4>.
- [34] D. Jacob, *Journal of Physics: Condensed Matter* **27**, 245606 (2015).
- [35] A. Droghetti, M. M. Radonjić, L. Chioncel, and I. Rungger, *Physical Review B* **106** (2022), URL <https://doi.org/10.1103/physrevb.106.075156>.
- [36] G. Gandus, A. Valli, D. Passerone, and R. Stadler, *The Journal of Chemical Physics* **153**, 194103 (2020), URL <https://doi.org/10.1063/5.0021821>.
- [37] P.-O. Löwdin, *The Journal of Chemical Physics* **18**, 365 (1950).
- [38] E. Pavarini, S. Biermann, A. Poteryaev, A. Lichtenstein, A. Georges, and O. Andersen, *Physical Review Letters* **92**, 176403 (2004).
- [39] I. Solov'yev, *Physical Review B* **69**, 134403 (2004).
- [40] T. Miyake, F. Aryasetiawan, and M. Imada, *arXiv preprint arXiv:0906.1344* (2009).
- [41] F. Aryasetiawan, K. Karlsson, O. Jepsen, and U. Schönberger, *Physical Review B* **74**, 125106 (2006).
- [42] A. Georges, G. Kotliar, W. Krauth, and M. J. Rozenberg, *Reviews of Modern Physics* **68**, 13 (1996), URL <https://doi.org/10.1103/revmodphys.68.13>.
- [43] S. Florens, *Physical Review Letters* **99**, 046402 (2007).
- [44] M. Snoek, I. Titvinidze, C. Töke, K. Byczuk, and W. Hofstetter, *New Journal of Physics* **10**, 093008 (2008), URL <https://doi.org/10.1088/1367-2630/10/9/093008>.
- [45] A. Valli, G. Sangiovanni, O. Gunnarsson, A. Toschi, and K. Held, *Physical Review Letters* **104** (2010), URL <https://doi.org/10.1103/physrevlett.104.246402>.
- [46] A. Valli, H. Das, G. Sangiovanni, T. Saha-Dasgupta, and K. Held, *Physical Review B* **92** (2015), URL <https://doi.org/10.1103/physrevb.92.115143>.
- [47] D. Jacob, K. Haule, and G. Kotliar, *Physical Review B* **82** (2010), URL <https://doi.org/10.1103/physrevb.82.195115>.
- [48] H. Bruus and K. Flensberg, *Many-body quantum theory in condensed matter physics: an introduction* (OUP Oxford, 2004).
- [49] E. Gull, A. J. Millis, A. I. Lichtenstein, A. N. Rubtsov, M. Troyer, and P. Werner, *Reviews of Modern Physics* **83**, 349 (2011), URL <https://doi.org/10.1103/revmodphys.83.349>.
- [50] M. Jarrell and J. Gubernatis, *Physics Reports* **269**, 133 (1996), URL [https://doi.org/10.1016/0370-1573\(95\)00074-7](https://doi.org/10.1016/0370-1573(95)00074-7).
- [51] Note1, this approximation neglects non-local interaction terms, which could otherwise be taken into account either at the mean-field level or within alternative implementations, such as extended DMFT [?].
- [52] H. Das, G. Sangiovanni, A. Valli, K. Held, and T. Saha-Dasgupta, *Physical Review B* **107** (2011), URL <https://doi.org/10.1103/physrevlett.107.197202>.
- [53] C. M. Kropf, A. Valli, P. Franceschini, G. L. Celardo, M. Capone, C. Giannetti, and F. Borgonovi, *Physical Review B* **100** (2019), URL <https://doi.org/10.1103/physrevb.100.035126>.
- [54] K. Baumann, A. Valli, A. Amaricci, and M. Capone, *Physical Review A* **101** (2020), URL <https://doi.org/10.1103/physrevb.100.075118>.

- 10.1103/physreva.101.033611.
- [55] A. Amaricci, A. Valli, G. Sangiovanni, B. Trauzettel, and M. Capone, *Physical Review B* **98** (2018), URL <https://doi.org/10.1103/physrevb.98.045133>.
 - [56] V. I. Anisimov, J. Zaanen, and O. K. Andersen, *Phys. Rev. B* **44**, 943 (1991), URL <https://link.aps.org/doi/10.1103/PhysRevB.44.943>.
 - [57] M. Czyżyk and G. Sawatzky, *Physical Review B* **49**, 14211 (1994).
 - [58] M. Karolak, G. Ulm, T. Wehling, V. Mazurenko, A. Poteryaev, and A. Lichtenstein, *Journal of Electron Spectroscopy and Related Phenomena* **181**, 11 (2010), URL <https://doi.org/10.1016/j.elspec.2010.05.021>.
 - [59] G. Kotliar, S. Y. Savrasov, K. Haule, V. S. Oudovenko, O. Parcollet, and C. A. Marianetti, *Rev. Mod. Phys.* **78**, 865 (2006), URL <https://link.aps.org/doi/10.1103/RevModPhys.78.865>.
 - [60] K. Held, *Advances in Physics* **56**, 829 (2007), URL <https://doi.org/10.1080/00018730701619647>.
 - [61] V. I. Anisimov, F. Aryasetiawan, and A. Lichtenstein, *Journal of Physics: Condensed Matter* **9**, 767 (1997).
 - [62] A. Petukhov, I. Mazin, L. Chioncel, and A. Lichtenstein, *Physical Review B* **67**, 153106 (2003).
 - [63] A. Liechtenstein, V. I. Anisimov, and J. Zaanen, *Physical Review B* **52**, R5467 (1995).
 - [64] V. I. Anisimov, I. Solovyev, M. Korotin, M. Czyżyk, and G. Sawatzky, *Physical Review B* **48**, 16929 (1993).
 - [65] I. Solovyev, P. Dederichs, and V. Anisimov, *Physical Review B* **50**, 16861 (1994).
 - [66] S. Datta, *Quantum transport: atom to transistor* (Cambridge university press, 2005).
 - [67] D. A. Ryndyk et al., *Springer Series in Solid-State Sciences* **184** (2016).
 - [68] G. Gandus, Y. Lee, L. Deusche, D. Passerone, and M. Luisier, *Solid-State Electronics* **199**, 108499 (2023), URL <https://doi.org/10.1016/j.sse.2022.108499>.
 - [69] Y. Meir and N. S. Wingreen, *Physical Review Letters* **68**, 2512 (1992).
 - [70] M. Rumetshofer, D. Bauernfeind, E. Arrigoni, and W. von der Linden, *Physical Review B* **99**, 045148 (2019).
 - [71] A. Ferretti, A. Calzolari, R. Di Felice, and F. Manghi, *Physical Review B* **72**, 125114 (2005).
 - [72] T.-K. Ng, *Physical Review Letters* **76**, 487 (1996).
 - [73] N. Sergueev, Q.-f. Sun, H. Guo, B. Wang, and J. Wang, *Physical Review B* **65**, 165303 (2002).
 - [74] A. Droghetti, M. M. Radonjić, A. Halder, I. Rungger, and L. Chioncel, *Physical Review B* **105** (2022), URL <https://doi.org/10.1103/physrevb.105.115129>.
 - [75] A. H. Larsen, J. J. Mortensen, J. Blomqvist, I. E. Castelli, R. Christensen, M. Dulak, J. Friis, M. N. Groves, B. Hammer, C. Hargus, et al., *Journal of Physics: Condensed Matter* **29**, 273002 (2017), URL <http://stacks.iop.org/0953-8984/29/i=27/a=273002>.
 - [76] J. J. Mortensen, L. B. Hansen, and K. W. Jacobsen, *Phys. Rev. B* **71**, 035109 (2005), URL <https://link.aps.org/doi/10.1103/PhysRevB.71.035109>.
 - [77] A. H. Larsen, M. Vanin, J. J. Mortensen, K. S. Thygesen, and K. W. Jacobsen, *Phys. Rev. B* **80**, 195112 (2009), URL <https://link.aps.org/doi/10.1103/PhysRevB.80.195112>.
 - [78] J. Enkovaara, C. Rostgaard, J. J. Mortensen, J. Chen, M. Dulak, L. Ferrighi, J. Gavnholt, C. Glinsvad, V. Haikola, H. A. Hansen, et al., *Journal of Physics: Condensed Matter* **22**, 253202 (2010).
 - [79] J. P. Perdew, K. Burke, and M. Ernzerhof, *Phys. Rev. Lett.* **77**, 3865 (1996), URL <https://link.aps.org/doi/10.1103/PhysRevLett.77.3865>.
 - [80] K. B. Clark, P. N. Culshaw, D. Griller, F. P. Lossing, J. A. M. Simoes, and J. C. Walton, *The Journal of Organic Chemistry* **56**, 5535 (1991), URL <https://doi.org/10.1021/jo00019a012>.
 - [81] N. Chalyavi, G. B. Bacskey, A. S. Menon, T. P. Troy, N. J. L. K. Davis, L. Radom, S. A. Reid, and T. W. Schmidt, *The Journal of Chemical Physics* **135**, 124306 (2011), URL <https://doi.org/10.1063/1.3640475>.
 - [82] C. Herrmann, G. C. Solomon, and M. A. Ratner, *The Journal of Chemical Physics* **134**, 224306 (2011), URL <https://doi.org/10.1063/1.3598519>.
 - [83] U. Fano, *Physical Review* **124**, 1866 (1961), URL <https://doi.org/10.1103/physrev.124.1866>.
 - [84] A. E. Miroshnichenko, S. Flach, and Y. S. Kivshar, *Reviews of Modern Physics* **82**, 2257 (2010), URL <https://doi.org/10.1103/revmodphys.82.2257>.
 - [85] Y. Zheng, P. Duan, Y. Zhou, C. Li, D. Zhou, Y. Wang, L.-C. Chen, Z. Zhu, X. Li, J. Bai, et al., *Angewandte Chemie International Edition* **61** (2022), URL <https://doi.org/10.1002/anie.202210097>.
 - [86] C. R. Arroyo, S. Tarkuc, R. Frisenda, J. S. Seldenthuis, C. H. M. Woerde, R. Eelkema, F. C. Grozema, and H. S. J. van der Zant, *Angewandte Chemie* **125**, 3234 (2013), URL <https://doi.org/10.1002/ange.201207667>.
 - [87] G. Yang, H. Wu, J. Wei, J. Zheng, Z. Chen, J. Liu, J. Shi, Y. Yang, and W. Hong, *Chinese Chemical Letters* **29**, 147 (2018), URL <https://doi.org/10.1016/j.cclet.2017.06.015>.
 - [88] Y. Li, M. Buerkle, G. Li, A. Rostamian, H. Wang, Z. Wang, D. R. Bowler, T. Miyazaki, L. Xiang, Y. Asai, et al., *Nature Materials* **18**, 357 (2019), URL <https://doi.org/10.1038/s41563-018-0280-5>.
 - [89] P. Sautet and C. Joachim, *Chemical Physics Letters* **153**, 511 (1988), URL [https://doi.org/10.1016/0009-2614\(88\)85252-7](https://doi.org/10.1016/0009-2614(88)85252-7).
 - [90] G. C. Solomon, D. Q. Andrews, T. Hansen, R. H. Goldsmith, M. R. Wasielewski, R. P. V. Duyne, and M. A. Ratner, *The Journal of Chemical Physics* **129**, 054701 (2008), URL <https://doi.org/10.1063/1.2958275>.
 - [91] P. Sam-ang and M. G. Reuter, *New Journal of Physics* **19**, 053002 (2017), URL <https://doi.org/10.1088/1367-2630/aa6c23>.
 - [92] D. Nozaki and C. Toher, *The Journal of Physical Chemistry C* **121**, 11739 (2017), URL <https://doi.org/10.1021/acs.jpcc.6b11951>.
 - [93] S. Gunasekaran, J. E. Greenwald, and L. Venkataraman, *Nano Letters* **20**, 2843 (2020), URL <https://doi.org/10.1021/acs.nanolett.0c00605>.
 - [94] Y.-F. Zhou, W.-Y. Chang, J.-Z. Chen, J.-R. Huang, J.-Y. Fu, J.-N. Zhang, L.-Q. Pei, Y.-H. Wang, S. Jin, and X.-S. Zhou, *Nanotechnology* **33**, 095201 (2021), URL <https://doi.org/10.1088/1361-6528/ac3b84>.
 - [95] J. Prasongkit and A. R. Rocha, *RSC Advances* **6**, 59299 (2016).
 - [96] O. Sengul, J. Völkle, A. Valli, and R. Stadler, *Phys. Rev. B* **105**, 165428 (2022), URL <https://link.aps.org/doi/10.1103/PhysRevB.105.165428>.

- org/doi/10.1103/PhysRevB.105.165428.
- [97] T. T. Phùng, R. Peters, A. Honecker, G. T. de Laisardière, and J. Vahedi, *Physical Review B* **102** (2020), URL <https://doi.org/10.1103/physrevb.102.035160>.
 - [98] S. Mishra, D. Beyer, K. Eimre, S. Kezilebieke, R. Berger, O. Gröning, C. A. Pignedoli, K. Müllen, P. Liljeroth, P. Ruffieux, et al., *Nature nanotechnology* **15**, 22 (2020).
 - [99] I. Alcón, G. Calogero, N. Papior, A. Antidormi, K. Song, A. W. Cummings, M. Brandbyge, and S. Roche, *Journal of the American Chemical Society* **144**, 8278 (2022), URL <https://doi.org/10.1021/jacs.2c02178>.
 - [100] L. Hedin, *Physical Review* **139**, A796 (1965), URL <https://doi.org/10.1103/physrev.139.a796>.
 - [101] F. Aryasetiawan and O. Gunnarsson, *Reports on Progress in Physics* **61**, 237 (1998), URL <https://doi.org/10.1088/0034-4885/61/3/002>.
 - [102] A. Stan, N. E. Dahlen, and R. van Leeuwen, *Europhysics Letters (EPL)* **76**, 298 (2006), URL <https://doi.org/10.1209/epl/i2006-10266-6>.
 - [103] J. B. Neaton, M. S. Hybertsen, and S. G. Louie, *Physical Review Letters* **97** (2006), URL <https://doi.org/10.1103/physrevlett.97.216405>.
 - [104] K. S. Thygesen and A. Rubio, *The Journal of Chemical Physics* **126**, 091101 (2007), URL <https://doi.org/10.1063/1.2565690>.
 - [105] K. S. Thygesen and A. Rubio, *Physical Review B* **77** (2008), URL <https://doi.org/10.1103/physrevb.77.115333>.
 - [106] C. Rostgaard, K. W. Jacobsen, and K. S. Thygesen, *Physical Review B* **81** (2010), URL <https://doi.org/10.1103/physrevb.81.085103>.
 - [107] M. Strange, C. Rostgaard, H. Häkkinen, and K. S. Thygesen, *Physical Review B* **83** (2011), URL <https://doi.org/10.1103/physrevb.83.115108>.
 - [108] M. Mansouri, D. Casanova, P. Koval, and D. Sánchez-Portal, *New Journal of Physics* **23**, 093027 (2021), URL <https://doi.org/10.1088/1367-2630/ac1bf3>.